Supplementary information to

Nanofluidic Resistive Pulse Sensing for Characterization of Extracellular Vesicles

Madalena R. C. Calado[a], Teresa C. Lage[a], Daniel A. M. André[a], Carlos Calaza[a], Carlos Marques[a], Carolina Herrero[b,c], João Piteira[a], Lars Montelius[a,d], Dmitri Y. Petrovykh[a], Lorena Diéguez[a]*, Alar Ainla[a]*

[a] International Iberian Nanotechnology Laboratory (INL), Braga, Portugal.
[b] Translational Medical Oncology Group (Oncomet), Health Research Institute of Santiago de Compostela (IDIS), University Hospital of Santiago de Compostela (SERGAS), Santiago de Compostela, Spain.
[c] Nasasbiotech, S.L., A Coruña, Spain.
[d] *Current affiliation:* Lund University, Lund, Sweden.

*Corresponding authors: lorena.dieguez@inl.int, alar.ainla@inl.int

Contents

1. Nanopore chip design

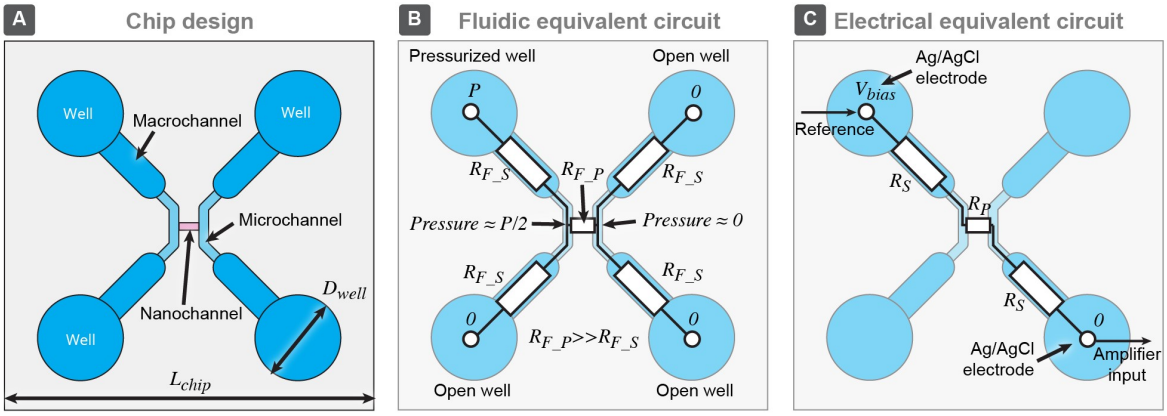

Figure S1. Nanopore chip design. (A) Chip is composed of three types of channels i) nanochannels, ii) microchannel and iii) macrochannels. Geometries of channels are described in Table S1 below. (B) Equivalent circuit diagram of fluidic resistances for the pressure driven flow mode, where R_{F_S} and R_{F_P} are the fluidic resistances of supply channels and nanochannels respectively. (C) Electric circuit diagram of the chip during two electrode RPS measurements, where R_S and R_P are electrical resistances of the supply -and nanochannels.

Table S1. Dimensions of channel types.

Channel	Length (µm)	Width (µm)	Height (µm)
Nanochannel	15	Variable (see Figure 2 main text)	1
Microchannel	200	20	15.4
Macrochannel	5000	300	95

2. Electrical and fluidic characteristics of the chip

Fluidic (hydrodynamic) resistance R_F of rectangular channels was calculated using equation eq.S1 below

$$R_F = \frac{12\eta L}{h^3 w\left[1 - \sum_{n,odd}^{\infty} \frac{192h}{n^5\pi^5 w} tanh\left(n\pi \frac{w}{2h}\right)\right]} \approx \frac{12\eta L}{h^3 w\left[1 - 0.630\frac{h}{w}\right]} \quad (eq.S1)$$

Where η is viscosity (in case of aqueous solutions here $\eta = 10^{-3} Pa\ s$), and L, w, h are channel, length width and height respectively.

Electrical resistance R of rectangular channels was calculated using equation eq. S2

$$R = \frac{L}{hw\sigma} \quad (eq.S2)$$

Where σ is specific conductivity of the buffer, in case of low (137mM) salt concentration $\sigma = 1.46 S/m$, while in case of high (1M) salt concentration $\sigma = 3.45 S/m$. For the calculation of electrical resistance of nanochannels with constrictions (pores) it is also important to separately consider the expansion zone, where channel expands from small constriction to wider channel. Resistance of this region is described by eq. S3.

$$R = \frac{2}{\pi h\sigma} ln\left(\frac{w}{w_P}\right) \quad (eq.S3)$$

Where w and w_P are the width of the wider nanochannel and pore constriction respectively.

These calculations yield fluidic -and electrical resistances of chip elements as shown in table S2. As it can be seen, fluidic resistances of nanochannels are at least two orders of magnitude larger than supply channels (micro- and macrochannels). Therefore to calculate pressure-driven flow through the nanochannel, the resistances of the supply channels can be neglected and hydraulic pressures on the ends of the nanochannel would be $P/2$ and 0, giving pressure difference $P/2$.

Table S2. Electrical and fluidic characteristics of channels.

Channel	Fluidic resistance (Pa s/m³)	Electrical resistance low salt (LS) buffer (MΩ)	Electrical resistance high salt (HS) buffer (MΩ)
Nanochannel chip 1	$5.6x10^{16}$	3.4	1.4
Nanochannel chip 2	$4.3x10^{17}$	10	4.3
Nanochannel chip 3	$7.1x10^{16}$	3.4	1.4
Nanochannel chip 4	$2.2x10^{17}$	7.5	3.2
Nanochannel chip 5	$1.0x10^{17}$	4.9	2.1
Nanochannel chip 6	$2.2x10^{17}$	5.4	2.3
Microchannel	$1.2x10^{14}$	0.44	0.19
Macrochannel	$2.9x10^{11}$	0.12	0.051

Using electrical and fluidic resistances we can evaluate both electric field strength in pores as well as pressure driven flow. The electrical field strength can be calculated as following (eq.S4)

$$E = \frac{V}{hw_P R_{Total}\sigma} \quad (eq.S4)$$

Where V, R_{Total} are electrical bias voltage and total resistance ($R_{Total} = 2R_S + R_P$). From the electrical field strength (which would be here in the range from 500 to 17´000V/m) electro-osmotic flow (EOF) can be found as $v_{EOF} = \mu_{EOF}E$, where μ_{EOF} is electro-osmotic mobility[1] (expected value for given materials would be around $\mu_{EOF} = 1.5 \cdot 10^{-8}\ m^2/V \cdot s$). In addition to EOF particles, while exposed to electric field, will also move electrophoretically (EP). Electrophoretic motilities of the particles were found during zeta potential measurement in low-salt conditions and was $\mu_{EP} = -1.19 \pm 0.27 \cdot 10^{-8}\ m^2/V \cdot s$. Thus EOF and EP are in the similar order of magnitude, but in opposite direction. On the other hand pressure driven flow would provide orders of magnitude faster particle transport compare to EOF and EP (Table S3)

Table S3. Electrical and fluidic characteristics of channels.

Channel	Electro-osmotic flow (EOF) low salt buffer at V=100mV (mm/s)	Electro-osmotic flow (EOF) high salt buffer at V=30mV (mm/s)	Pressure driven flow velocity at p=100mbar (mm/s)
Nanochannel chip 1	0.26	0.033	146
Nanochannel chip 2	0.062	0.0078	12
Nanochannel chip 3	0.26	0.033	118
Nanochannel chip 4	0.16	0.021	46
Nanochannel chip 5	0.12	0.015	48
Nanochannel chip 6	0.21	0.027	46

3. Fabrication of the chip

Method S1 (Master mold). The master to create microfluidic devices was fabricated by INL cleanroom facility using 200mm 725µm thick Si wafers as a substrate. The master included three layers:

Nanochannel layer: A layer of 300nm of SiO_2 was deposited on the wafer using SPTS PECVD system. Then the wafer was plasma treated in Tepla Plasma Asher with a mild O_2/Ar plasma and vapour primed with HDMS, followed by spin-coating of 200nm of diluted e-beam resist ARN7520 (Allresists GmbH) using Suss Microtec Gamma Cluster automated spin-coating system. The resist was exposed using Vistec 5200 ES 100 kV e-beam lithography system with 15nA current, 10nm pixel size and 640 µC/cm^2 dose settings. Thereafter the wafer was post-exposure baked at 85 ºC for 120s and developed with AR 300-47 using Suss Microtec Gamma Cluster. After optical and SEM inspection the SiO_2 was etched in SPTS APS system. The resist was then striped in Tepla Plasma Asher and the patterns on the SiO_2 hard mask were transferred into the silicon substrate with a SPTS Pegasus DRIE etcher using the pseudo-Bosch process (etch thickness 1µm). Finally the remaining SiO_2 hard mask was removed in a SPTS Primaxx – HF Vapor Etcher and remaining etch residues were cleaned in a EKC 265 heated bath.

Microchannel layer: The wafer with nanochannels was treated with a mild oxygen plasma in SPTS Pegasus for surface activation. Channels were fabricated in SU-8 2010 using standard process parameters: spin-coating at 1500rpm for 30s for a 15µm target thickness, soft-baking, exposure in mask aligner MA6 (Karl Suss), post exposure baking, development at SU-8 developer and rinsing with IPA using spin-coater. Completed structures were hard baked at 150 ºC oven (Memmert) for 10min with slow 2h ramping. Final resist thickness was characterized with mechanical profile KLA Tencor P-16+.

Macrochannel layer: The wafer with nanochannels and microchannels was treated with a mild oxygen plasma in SPTS Pegasus for surface activation. Channels were fabricated in SU-8 2050 using standard process parameters: spin-coating at 1600rpm for 30s for 110µm target thickness, soft-baking, exposure in mask aligner MA6 (Karl Suss), post exposure baking, development at SU-8 developer and rinsing with IPA using spin-coater. Completed structures were hard baked at 150 ºC oven (Memmert) for 8h with slow 4h ramping. Final resist thickness was characterized with mechanical profile KLA Tencor P-16+.

Completed wafer was inspected optically (Nikon Eclipse L200N) and with SEM (FEI NovaNano). Eventually the wafer was surface treated in a desiccator using 1H,1H,2H,2H-perfluorooctyldimethylchlorosilane to avoid PDMS adhesion.

Method S2 (Nanopore chip fabrication). All chips were fabricated using a single master mold wafer (Method S1). All fabrication was performed at standard chemical laboratory settings. First two silicone mixtures were prepared. Softer (sPDMS) was prepared by mixing Sylgard™ 184 silicon elastomer kit components in ratio 1:10 (w/w). Harder (hPDMS) was prepared by first mixing GELEST® hPDMS high modulus reprographic silicone components 1:1 (w/w), then this mixture was further mixed with sPDMS mixture in the ratio 1:1 (w/w). Both mixtures were placed to vacuum desiccator to remove bubbles. Small amount of hPDMS mixture (~1 µL) was spotted to the nanochannel areas on the master mold and cured at oven at 65 ºC for 30min, after which all wafer was covered with 5mm layer of sPDMS mixture and cured at 65 ºC for at least 12h. Then the PDMS slab was peeled from the master. Liquid wells were created using 3mm biopsy bunch and finally the slab was cut into 32 individual chips. PDMS pieces and glass microscopy slides were placed to Plasma Cleaner (ODC-002-CE, Harrick Plasma) and treated with oxygen plasma for 1min. Then we aligned and bonded PDMS and glass. Bonding was completed at 65 ºC oven for >2min. To maintain channels hydrophilic chips were loaded with water solution of Pluronic F-127 (Sigma-Aldrich) 0.1% (w/v) and wells were covered with tape, after which devices were stored in humidified container in fridge until used.

Method S3 (Ag/AgCl electrodes). For electrical readout, the chip was interfaced with Silver-Silver Chloride (Ag/AgCl) electrodes placed into the wells. We prepared electrodes using electrochemical

oxidation of Ag wire in HCl solution. Briefly a silver wire (0.5mm diameter) was polished with sandpaper and rinsed with water. Thereafter wire was submerged into 0.1M HCl with platinum counter electrode. Ag wire was connected as an anode and Pt wire as a cathode and current density 10mA/cm^2 was applied for 1min. Resulting Ag/AgCl layer had mat white to grey colour.

4. Data processing algorithm

4.1 Overview of the algorithm

Data processing algorithm was developed in MATLAB R2018b, it would automatically load and process data using settings, which user can define. User can preview the processing (e.g. detected spikes on the raw signal) to ensure that settings are optimal for given signal and adjust the settings, if desirable. The algorithm and the data processing workflow is illustrated on figure S2 below. Values are exemplified on table S4.

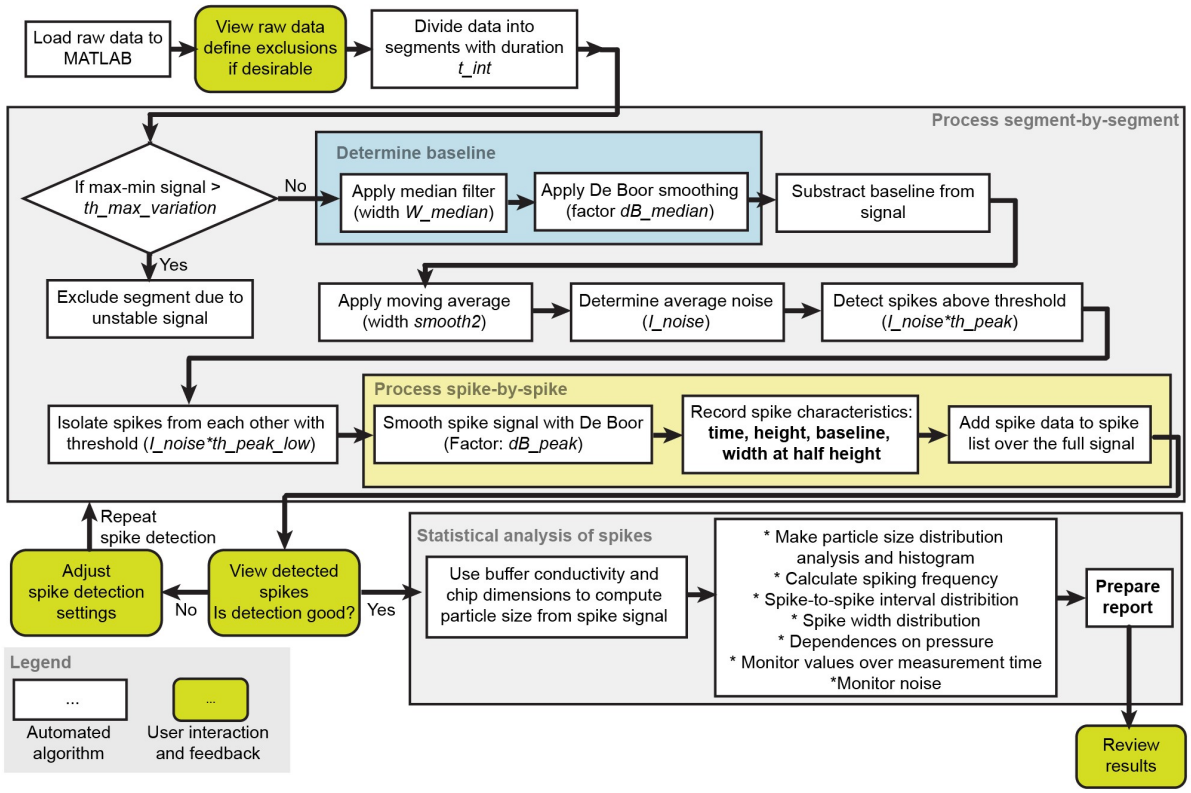

Figure S2. Flow diagram of the data processing with algorithm and user feedback.

Table S4. Typical range of values for the parameters of the algorithm used for data processing here.

Characteristic	Symbol	Typical value range	Unit
Duration of segments	*t_int*	~1	s
Maximum allowed signal variation in one segment	*th_max_variation*	0.25…10	nA
Median filter width for baseline	*w_median*	200*	dps
De Boor smoothing factor for baseline	*dB_median*	0.9995	
Moving average width (Applied after the baseline correction)	*smooth2*	1	dps
Spike threshold (relative to average noise)	*th_peak*	3…4	x noise
Spike base threshold (relative to average noise)	*th_peak_low*	0.25…0.5	x noise
De Boor spike smoothing factor	*dB_peak*	0.9999995	

* - it is corresponding to 10ms in case of typical sampling rate of 20kHz.

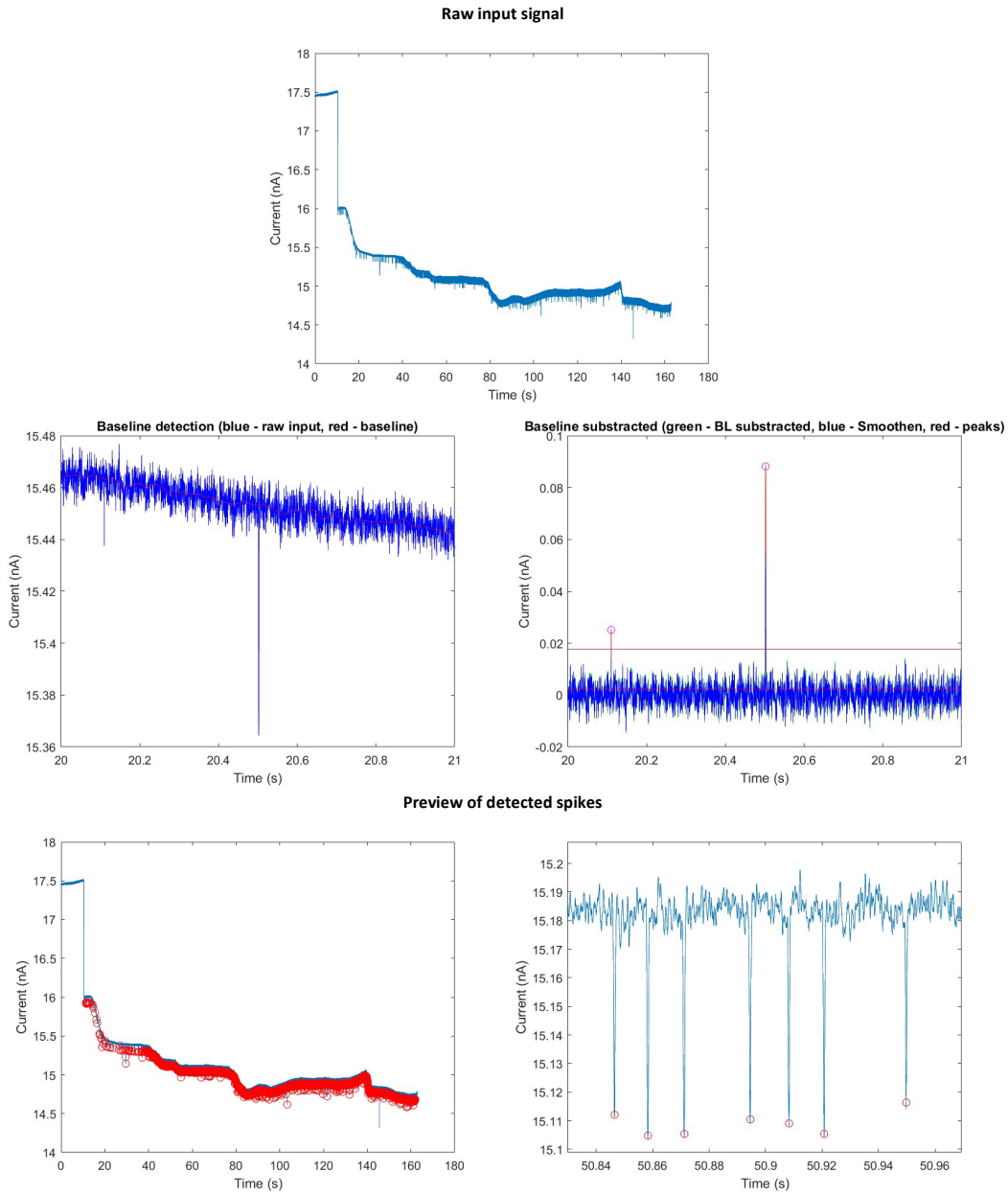

Figure S3. Exemplary illustration of spike detection process. (Top) Raw input signal. (Middle left) baselines detection in 1s segment, where blue is the raw signal and red is detected baseline. (Middle right) baseline corrected signal. Upper red line indicates the spike detection threshold (4x the noise level) and lower red line is the peak base threshold (0.5 x the noise level), signal has to go above the first to be considered as spike and drop below the second between two spikes, for them to be considered as individual. Pink circle marks detected peak height and location and red peak is the top half of the spike which defines also the spike width. (Bottom) Final review of fully processed signal with detected spikes (left), where user can zoom in to inspect the quality of the result (right).

4.2. Example of the reported analysis result

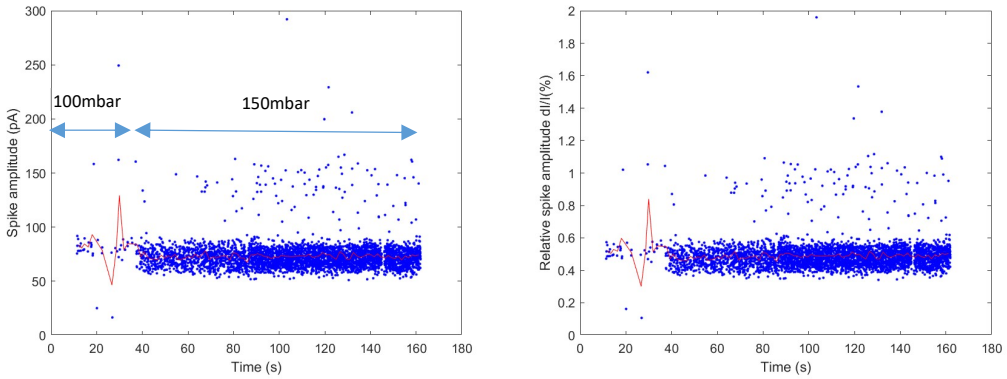

Figure S4. Spike amplitude absolute (left) and relative (over baselines) (right). Blue dots are individual spikes, green dots are excluded regions, and red line represent average trend.

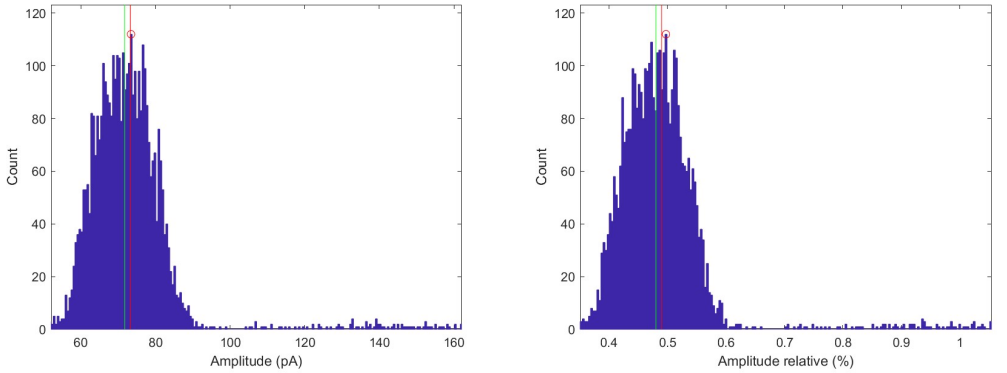

Figure S5. Spike amplitude histograms absolute (left) and relative (right). Red line is mean, green line is median, red circle is max expected value. Most expected values are I: 73.42 pA or I_{rel}: 0.50 %

Spike statistics:

Total number of spikes detected N: 3956
In following statistical analysis excluded regions are removed
Total number of spikes included in statistics N: 3956

Absolute values

Mean amplitude: 73.26 pA
Median amplitude: 71.75 pA
Standard deviation: 13.96 pA
Variation (std/mean): 19.06 %

Relative values

Mean amplitude: 0.49 %
Median amplitude: 0.48 %
Standard deviation: 0.093 %
Variation (std/mean): 19.0 %

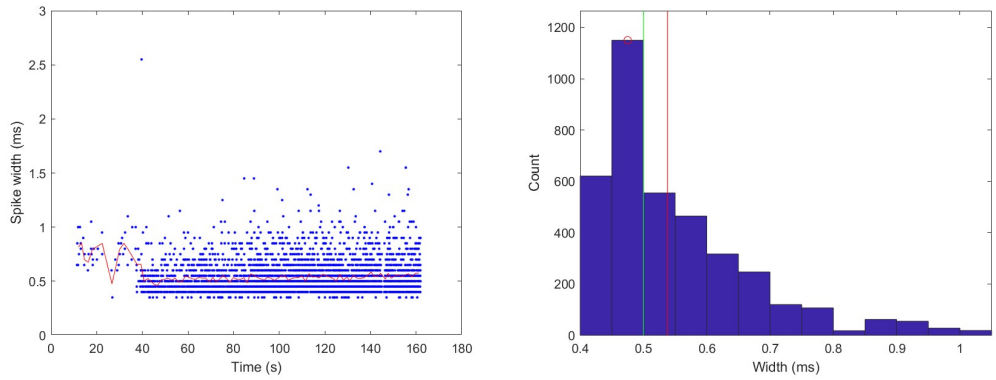

Figure S6. Spike width depending on time (left) and spike width distribution histogram (right). Red line is mean, green line is median, red circle is max expected value. Most expected value is w: 0.48 ms.

<u>Spike width analysis:</u>
Mean amplitude: 0.54 ms
Median amplitude: 0.5 ms
Standard deviation: 0.150 ms
Variation (std/mean): 27.8 %

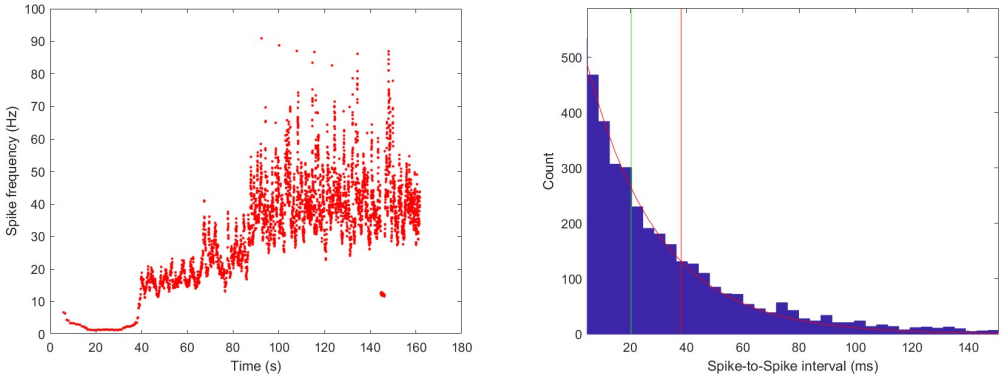

Figure S7. Average spike frequency (left) and spike-to-spike delay histogram (right). Red line is mean, green line is median. Red curve is expected exponential distribution for Poisson process. Most expected value is t: 2.68 ms. Mean frequency: 26.28 Hz.

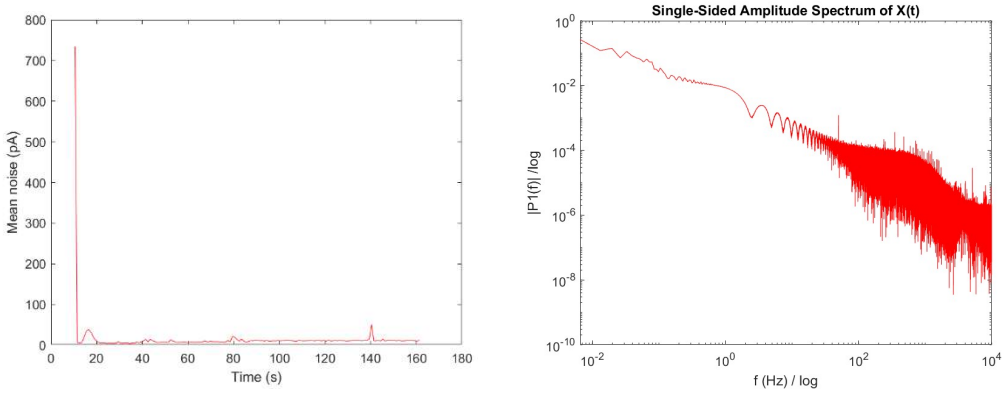

Figure S8. Noise. RMS noise over time (left) and noise spectrum (nA^2/Hz) of full recording (right). Max. noise in range 1 to 10 Hz: 1.00131 Hz, 0.0086 nA^2/Hz power

Max. noise in range 10 to 100 Hz: 50.0065 Hz, 0.0012 nA^2/Hz
Max. noise in range 100 to 1000 Hz: 350.059 Hz, 0.00036 nA^2/Hz
Max. noise in range 1000 to 10000 Hz: 1138.77 Hz, 9.81e-05 nA^2/Hz

5. Failure analysis

In order to evaluate quality of the obtained data and devices, we identified and categorized observed failure modes and how to detect and exclude them (Figure S8-S9). If nanopore had been mechanically damaged during the fabrication, this usually resulted in baseline current significantly out of the expected range or even current saturation of the amplifier, though also successful devices showed a variation of baseline current values (Figure S10). Other failures could be categorized: i) bubble entering the channel, ii) highly unstable and fluctuating baseline and iii) clogging. Even though clogging would usually not block the current substantially, it can be seen as stop of spiking or as an increase in spike duration and reduction of spiking frequency (Figure S9), while effect on the actual spike amplitude was often less noticeable. Sometimes clogging resolved by itself or with assistance of pressure. Time ranges, which presented features of clogging, could be excluded from the final statistics to improve the data quality.

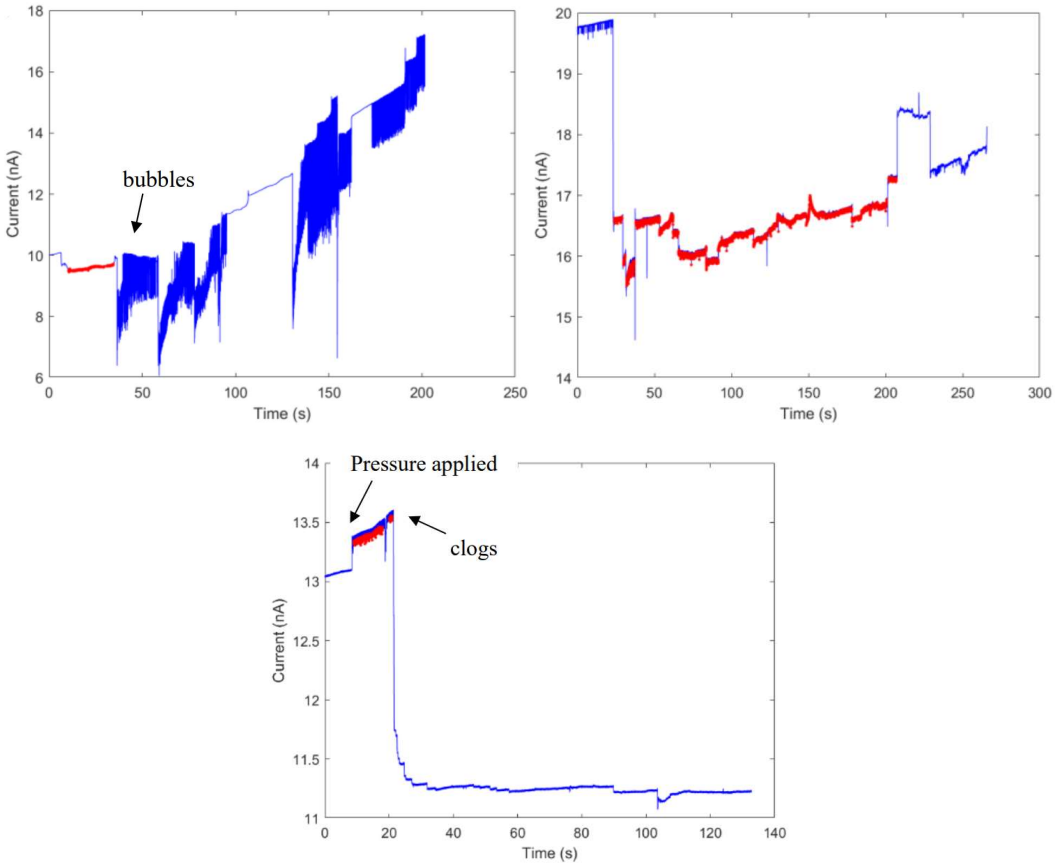

Figure S9. Observed failure modes in raw signal. (Top left) Bubbles seen as high frequency high amplitude oscillations. (Top right) Highly unstable baseline. (Bottom) Clogging, which represented as small drop in baseline current, but complete stop in spiking.

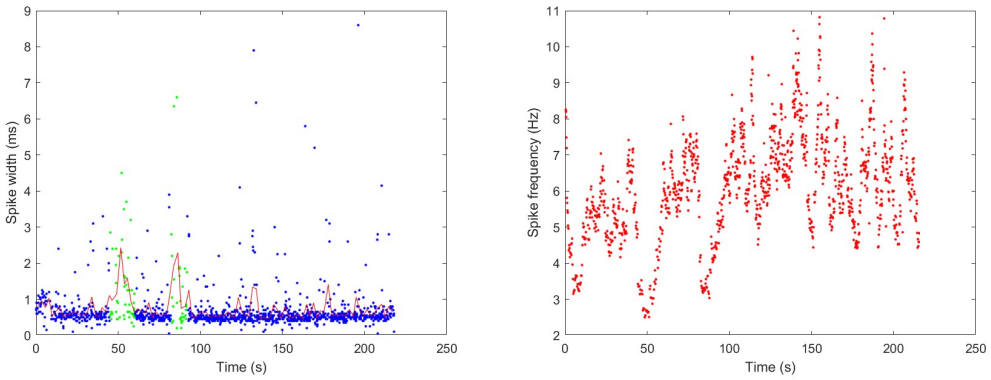

Figure S10. Determining partial clogging in the processed data. (Left) Temporal fluctuation in average spike width (red). When spikes are becoming in average longer, it is indicating particle clogging of the nanochannel (green marks spikes during clogging, which could be excluded from further analysis). This is also reflected in reduction of spiking frequency in similar ratios (Right).

6. In-house developed RPS data acquisition system

6.1. Design

For demonstration of compact and lower-cost readout alternative to the patch-clamp amplifier, we developed an in-house RPS data acquisition system. The key element of the data acquisition system is a low-noise analog front-end, comprising a trans-impedance amplifier (TIA) followed by a selectable post-gain stage, for increasing the overall gain without compromising overall bandwidth and noise performance. Our TIA was based on the OPA140 operational amplifier (Texas Instruments), featuring a low bias-current of 10pA and a low voltage-noise of 5.1nV/sqrt(Hz). The post-amplifier was based on the OPA2192 dual operational amplifier (Texas Instruments), featuring an offset-voltage of just 5µV and a low voltage-noise of 5.5nV/sqrt(Hz). The front-end had two selectable gains, 10MΩ and 40MΩ, giving a full-scale current of 400nA and 100nA, respectively. In order to reduce the noise from grid-connected power supplies, the analog electronics were powered by two 9V batteries. For electromagnetic shielding, the front-end together with the chip were placed inside of a shielding box made out of copper sheet. Electronics without the shielding box had significantly higher noise levels. Analog signal from the front-end was digitized with commercial data acquisition (DAQ) card DT9836 (Digilent, Pullman, WA) using QuickDAC software. We used one analog input (16-bit, maximum 225Ksps/s) to read the RPS signal and one analog output (16-bit) to configure the bias voltage. This DAQ card was chosen due to in-house availability and had significantly higher performance (many different input and output channels) and cost (~3300EUR) than actually needed here and could be later easily substituted with small and much lower-cost ADC and DAC chips connected to a microcontroller, in an embedded solution (Alternative options and costs are described in SI section 11).

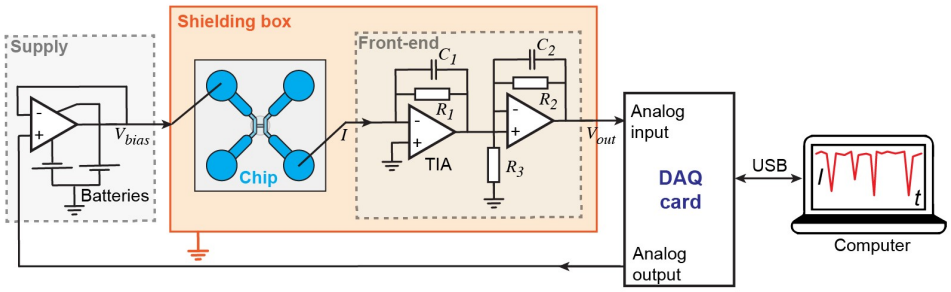

Figure S11. Conceptual design of in-house developed RPS data acquisition system.

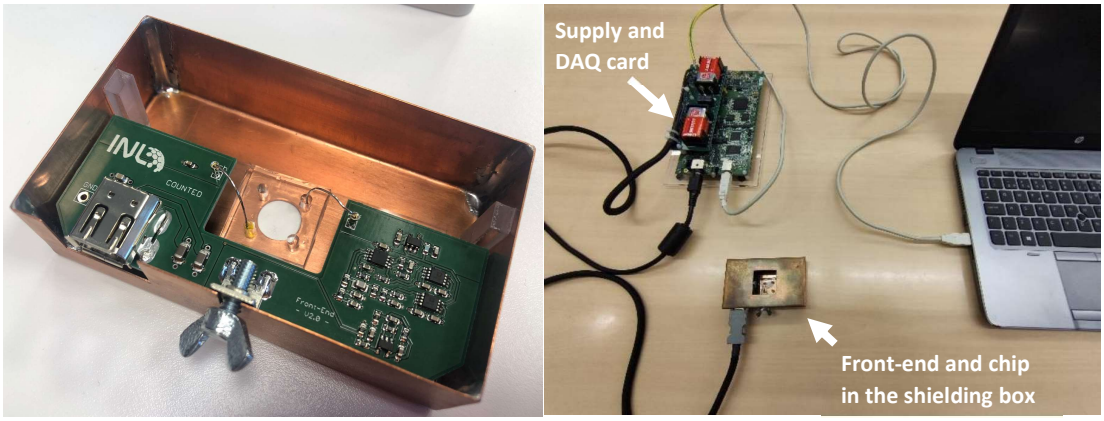

Figure S12. Photos of in-house built setup. (Left) analog front-end and shielding box (opened) with the nanopore chip interfaces with two Ag wire based Ag/AgCl electrodes. The shielding box had also openings for simultaneous microscopy imaging. (Right) Full setup including supply and DAQ card and laptop computer used for data logging.

6.2. Performance evaluation

We tested combinations of same chip type and particles on in-house developed device (left images) and commercial patch-clamp amplifier (right images), as exemplified on figures S12-S14 and summarized in tables S5.

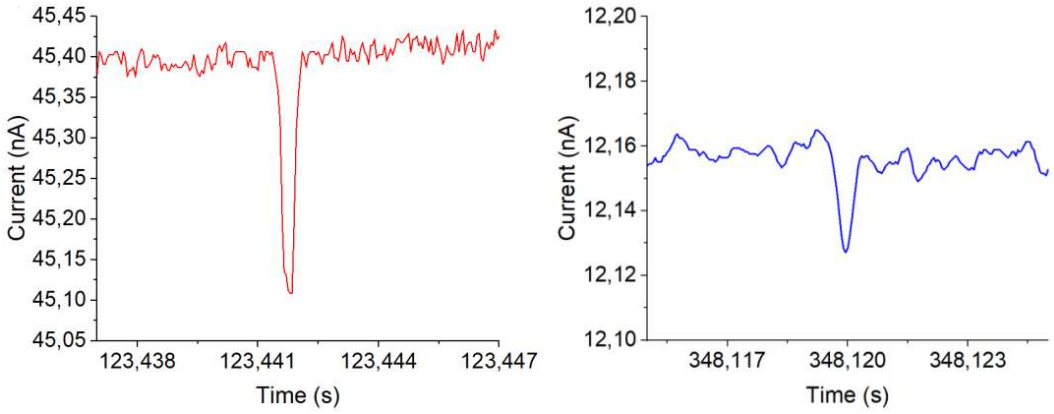

Figure S13. Comparison with Chip 2 (Smooth channel). 500nm particles (2.9 10^9 particles/mL), 1M PBS. In-house interface (left) and patch-clamp amplifier (right).

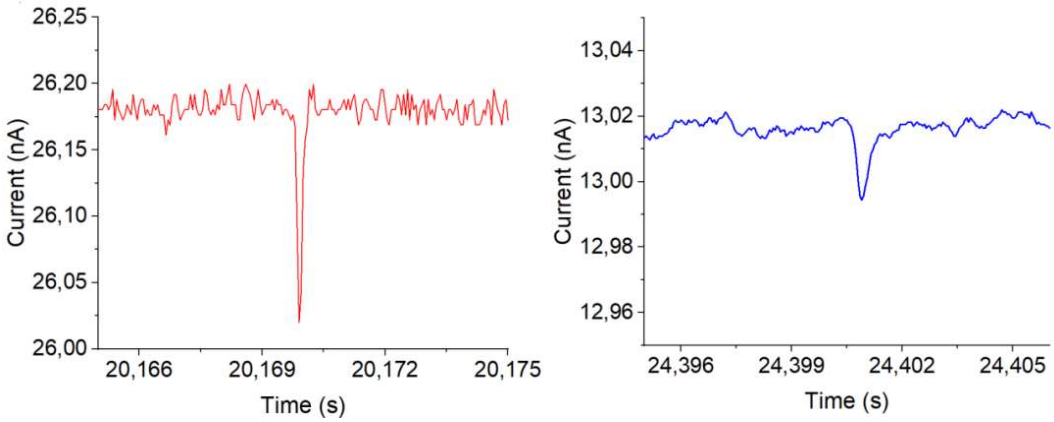

Figure S14. Comparison with Chip 6 (Single constriction). 230nm particles (2.5 10^{10} particles/mL), 0.137M PBS. In-house interface (left) and patch-clamp amplifier (right).

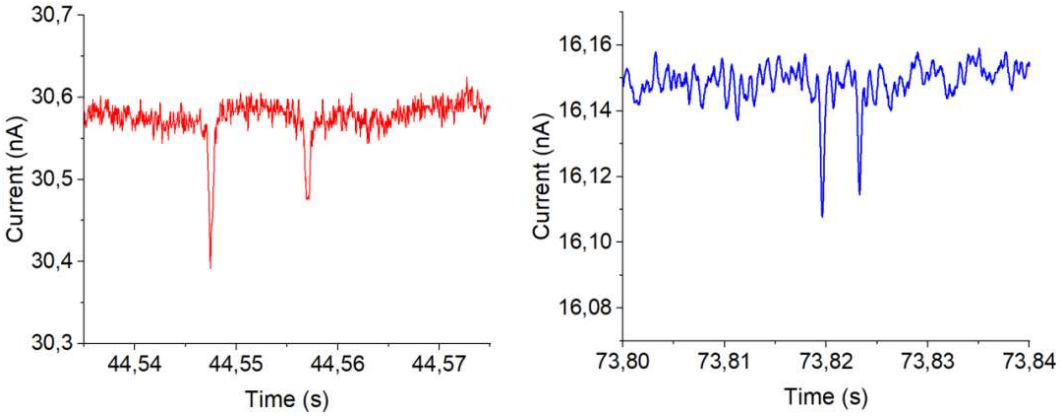

Figure S15. Comparison with Chip 4 (Double constriction). 230nm particles (2.5 10^{10} particles/mL), 1M PBS. In-house interface (left) and patch-clamp amplifier (right).

Table S5. Comparison of in-house constructed

Characteristic	In-house interface	Commercial Patch-Clamp amplifier
CHIP 2, 500nm particles, 2.9 10^9 particles/mL, 1M PBS, 200mbar		
Spiking frequency (Hz)	*50*	46
Spike height (pA)	*292±40*	65.7*±6.4*
Height variation (%)	*14*	18
Baseline (nA)	*45.14±0.51*	12.19*±0.13*
Noise (pA RMS)	*11*	3.1
Signal-to-noise ratio (SNR)	*27*	11
CHIP 5, 230nm particles, 2.5 10^{10} particles/mL, 0.137M PBS, 50mbar		
Spiking frequency (Hz)	*79*	41
Spike height (pA)	*156±90*	26*±11*
Height variation (%)	*57*	43
Baseline (nA)	*26.59±0.50*	13.04*±0.05*
Noise (pA RMS)	*7.8*	1.9
Signal-to-noise ratio (SNR)	*20*	14
CHIP 4, 230nm particles, 2.5 10^{10} particles/mL, 1M PBS, 100mbar		
Spiking frequency (Hz)	*11*	17
Spike height (pA)	*135±45*	41*±11*
Height variation (%)	*33*	27
Baseline (nA)	*29.5±1.1*	16.22*±0.06*
Noise (pA RMS)	*13*	4.0
Signal-to-noise ratio (SNR)	*11*	10

7. Pressure controller

Even though pressure driven mechanism needs a pressure generation, it could be compact and cost-effective element in the system, with principal components listed below in table S6. Bill of material would be less than 70 EUR.

Table S6. Principal components need to for a simple computer controlled pressure generator

Description	Supplier	Product code	Quantity	Unit price (EUR)
Miniature air pump kpm12a (3V)	Amazon.es	B00LUUKH98	1	9.99
Solenoid valve KSV05A-016 (3V)	Amazon.com	B0105UONPW	1	1.8
Pressure sensor ABPMANV015PG2A3, 0 to 15psi, I^2C, 3.3V	Mouser	785-ABPMANV015PG2A3	1	26.03
Transistor n-ch MOSFET LGE2302 (Q1 and Q2)	TME	LGE2302-LGE	2	0.05
Silicone tubing 2mm ID x 4mm OD, 2m	Amazon.es	B07SYY334B	1	8.8
Microcontroller board	Amazon.es	B06Y3ZHPWC	1	22.36

8. Methods for preparation and characterization of EVs samples

For testing purposes two sets of purified EVs samples were prepared and characterized independently in two different laboratories. Preparation and conventional characterization methods used for the EVs samples are described in following.

8.1. EVs sample 1

Method S4

EV from HCT116 cell line. The human colorectal cancer cell line HCT116 (ATCC, CCL-247), was maintained in McCoy's 5A culture medium (Gibco, Grand Island, NY, USA) supplemented with 1% penicillin-streptomycin (Gibco, Grand Island, NY, USA) and 10% FBS (Gibco, Thermo Fisher Scientific) reduced in EVs by ultracentrifugation for 16 hours at 4ºC, as described in Mariscal J. et al[2]. HCT116 cell line, was maintained in a humidified atmosphere at 37ºC and 5% CO_2. After 48 h, 38 ml of the conditioned culture medium was collected and EVs were isolated by differential centrifugation under the following conditions: 500g, 10 min; 10'000g, 20 min, 4ºC and ultracentrifugation at 100'000g, 16 h, 4ºC using a SW32Ti rotor (Beckman Coulter, Brea, CA, USA). EVs were resuspended in 500ul of DPBS and stored at -80ºC until use.

NTA analysis. The NTA uses the light scattering and Brownian motion to obtain measurements of concentration and size distribution of particles in a liquid suspension. EVs pellets obtained after isolation and resuspended in 500ul of DPBS, were resuspended in another 500 ul of DPBS and EVs concentration was measured by NTA system NanoSight NS300 (Marlvern, UK), equipped with a 405 nm wavelength laser. After capture, videos were analysed using NanoSight NTA 3.4.003 software with detection threshold of 17.

8.2. EVs sample 2

Method S5

Cell line and cell culture. Human endometrial adenocarcinoma cell line HEC-1A was cultured in McCoy's 5A media (Gilco, Grand Island, NY, USA) supplemented with 1% penicillin and streptomycin (Gilco, Grand Island, NY, USA) and 10% FBS (Gilco, Thermo Fisher Scientific) and maintained in a humidified incubator with 5% CO_2 at 37ºC. The cell line was routinely tested for mycoplasma. EVs collection was performed after culturing cells for 48h with medium with 10% of FBS reduced in EVs by ultracentrifugation during 16h at 4°C, as previously described[2].

Isolation of EVs by ultracentrifugation (UC). After collecting the conditioned media, EVs were harvested by differential centrifugation with the following conditions: 500g, 10 min; 10'000 g, 20 min, followed by ultracentrifugation at 110'000g, 16h or 2h, 4°C using OPTIMA XE-100 (Beckman Coulter, Brea, CA, USA). A washing step with dPBS (Gilco, Grand Island, NY, USA) was performed for 2h at 110'000g, 4°C. Pellets were resuspended in dPBS and stored at - 80°C.

Isolation of EVs by size exclusion chromatography (SEC). SEC was performed according to the manufacturer's instructions of the qEVoriginal 70 nm Gen 2 Columns (Izon, Christchurch, New Zealand). Briefly, 500 µl the EVs Pellet after UC 2h+2h and UC 16h was loaded on top of the qEV column and 4 fractions of 400 µl were collected using dPBS as an eluent.

Bicinchoninic acid assay (BCA assay). Protein concentration of EV samples was determined using Pierce™ BCA Protein Assay Kit (Thermo Fisher Scientific Inc., Waltham, MA, USA) according to the manufacturer's instructions.

NTA analysis. NTA was performed according to manufacturer's instructions using a Malvern Panalytical NanoSight NS300 (Malvern Instruments, Malvern, UK) configured with a Blue 488nm laser and a high-sensitivity sCMOS camera. The absence of background was verified using 0.2-µm-filtered Milli-Q water. For NTA analysis dPBS was used as a diluent, and five videos of 60 s were captured at

camera level 12 for UC 16h samples and 14 for UC 2h+2h samples. The videos were then analyzed using the NTA 3.0 software version (Malvern Instruments, Malvern, UK) with a detection threshold of 10.

RPS analysis. EVs sample 2 was evaluate with home-made electronics using bias voltage 200mV, 100nA (high gain) range and sample rate 100ksps. Higher sample rate compared to patch-clamp amplifier (20ksps) allowed more detailed measurement of pulse duration, which could be used to evaluate the flow velocity in the nanopore.

9. Additional characterization

9.1. Baseline resistance

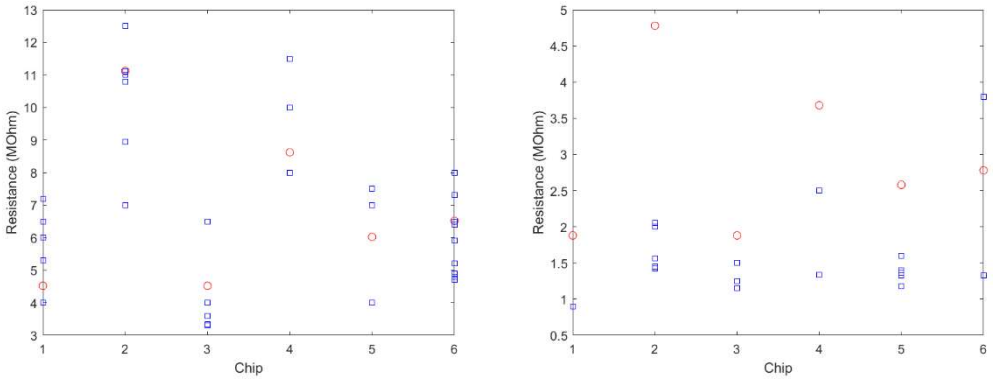

Figure S16. Baseline resistance values with low-salt (left) and high-salt (right). Red circles indicate theoretically calculated values, while blue squares are average measured values from different experiments. In case of high salt values appear consistently lower than expected.

9.2. NTA and DLS measurements of particle samples

NTA analysis of particles. For side-by-side comparison particle samples of various composition and concentration were evaluate also by NTA Malvern Panalytical NanoSight NS300 (Malvern Instruments, Malvern, UK). For consistency, experimental settings were first optimized and chosen values were kept constant as much as possible to avoid bias. Settings used: camera level: 14; gain: 1; continuous flowrate: 40; number of captures: 5; capture duration: 60s; detection threshold: 8; chamber cleaning: 5min between the samples. For 460nm particles the camera level had to be reduced to 8, since otherwise measurement was not be possible due to saturation.

DLS analysis of particles. Size of the particles was also evaluated by dynamic light scattering (DLS) using Zetasizer Nano (Malvern Instruments) dispersed in dPBS at room temperature using a 90° angle. Five measurements were performed for each sample and averaged, discarding values of measurements, which had polydispersity index above 1.

Measurement results are shown on figure S17. In case of optimal sample concentration (around 10^8/mL) good agreement of both size and concentration was obtained with manufacturer specified values, when single particles dilutions were measured. In case of mixtures, multimodal sample of 252nm and 460nm particles (in count ratio 1:1) could be still measured for concentration, but size distribution suffered significant distortions, where 250nm particles appeared correctly, while 460nm peak had shifted 100nm towards smaller sizes.

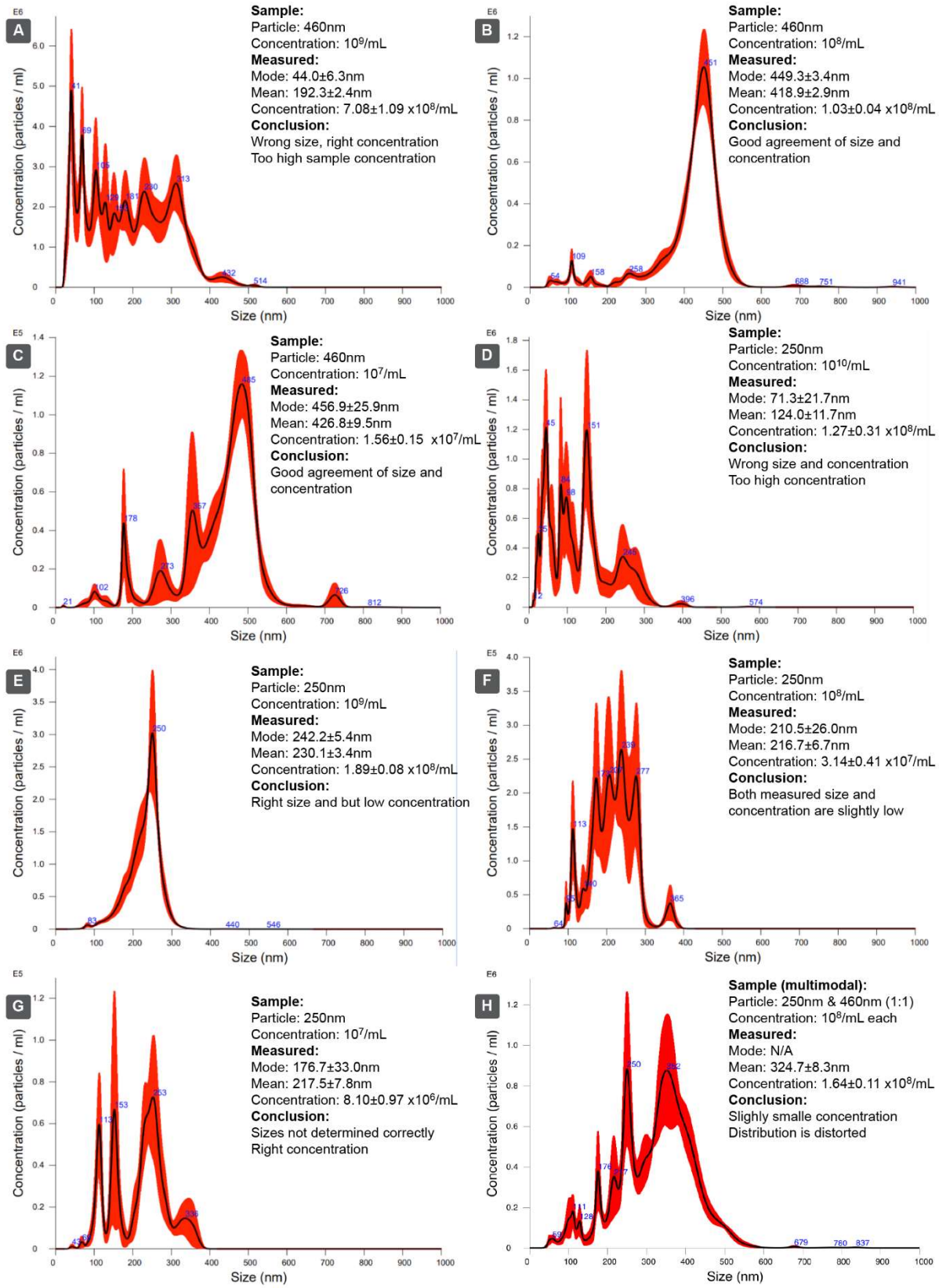

Figure S17. NTA measurement of samples of polystyrene test particles of 460nm and 250nm in different dilutions and as mixture for side-by-side assessment.

Table S7. DLS measurement of test particles for their size.

Particle size (nm)	Concentration (/mL)	Mean ± STD (nm)	Polydispersity index ± STD	Comment
460	10^{10}	175.4±5.7	0.3±0.2	Too high concentration
460	10^{9}	520±11	0.1±0.0	
460	10^{8}	476±40	0.2±0.1	Good agreement
460	10^{7}	463±34	0.3±0.2	Good agreement
250	10^{10}	229.5±9.7	0.2±0.1	
250	10^{9}	298.6±5.1	0.0±0.1	
250	10^{8}	304±23	0.2±0.2	
250	10^{7}	288±14	0.1±0.0	
250, 450	10^{8} both	513±11	0.1±0.1	Smaller particles are completely dismissed

9.3. Characteristics of EVs sample 2

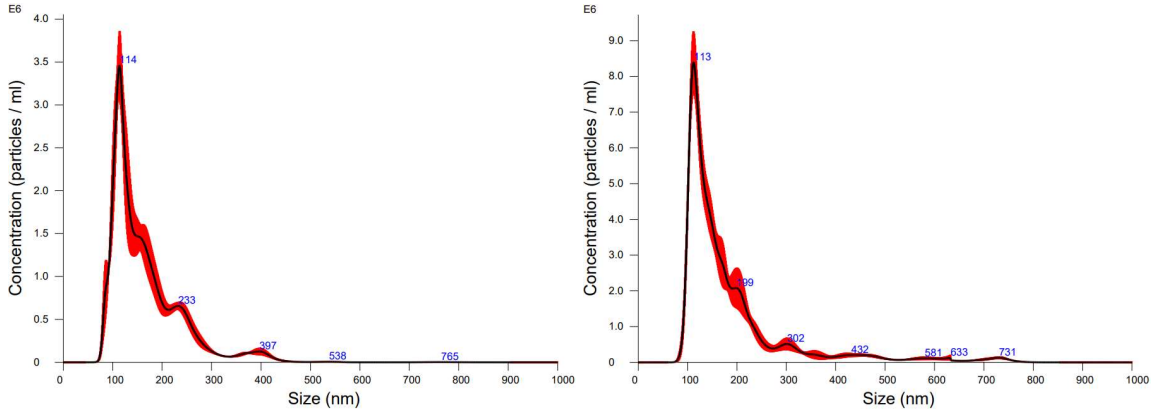

Figure S18. NTA measurement of EVs sample 2. On left after 16h UC diluted 20x and on right after SEC (fraction 1). Numerical characteristics of samples are described in table S8.

Table S8. Characterization of EVs sample 2 after different steps

Steps	Particle concentration (/mL) NTA	Protein content (µg/mL) BCA	Mean size (nm) NTA	Mode (nm) NTA	Comment
16h UC	5.14±0.28 x10^{9}	10362	164.1±2.2	112.8±3.6	High protein content
16h UC + 2h UC	5.48±0.19 x10^{9}	3972	157.7±1.2	106.4±2.8	2 step process reduces protein
16h UC + SEC (f1)	6.14±0.13 x10^{8}	< LOD	186±4.2	112.7±2.1	SEC very significantly removes protein contamination, but dilutes the sample

10. Cost of materials

This section describes the cost estimate of the RPS system, which has three parts: i) readout electronics for signal acquisition, ii) pressure controller and iii) consumable chip. The component cost of readout electronics is estimated in Table S9 below, which is below <120EUR for single device, but could be less than half of that in case of high volumes. Component cost of the pressure controller without the microcontroller, which could be shared with the readout electronics is <47EUR (further described in SI section 7), summing into total cost of the instrument below <170EUR. Purchase costs of materials required for the consumable PDMS chips is detailed in table S10, excluding initial fabrication cost of the re-usable master mold, which can be highly dependent on the particular facility performing the fabrication. Replication cost however is affordable (0.59EUR/chip).

Table S9. Analysis of exemplary component cost for implementation of readout electronics of the RPS system (BOM). Costs here considers necessary chips (Microcontroller, operational amplifiers, high-speed ADC, DAC) also to substitute the data acquisition (DAQ) card used in our laboratory prototype. Cost of the components is according public catalogue pricing as of 2024/06/19. Following sources were considered: electronic components from Mouser Electronics (https://mouser.com); PCB boards from EuroCircuits (for low-volume, https://www.eurocircuits.com) and PCBWay (for high-volume, https://www.pcbway.com);

Component	Exemplary value	Manufacturer/ Supplier	Qnt.	Low-volume cost (1 unit, EUR)	High-volume cost (1000 units, EUR/unit)
Precision operational amplifier for front-end	OPA140	Texas instruments	1	3.71	1.88
Precision operational amplifier.	OPA2192	Texas instruments	2	4.21	2.23
ADC, SPI interface, 16-bit and over 100ksp	MCP3461R	Microchip Technologies	1	2.21	1.67
DAC, 16-bit	DAC8551	Texas instruments	1	5.58	3.16
Microcontroller module, 32-bit with SPI and USB interfaces	XIAO ESP32C3	Seeed Studio	1	4.64	4.64
LDO (+5V)	MCP1824T-5002	Microchip Technologies	1	0.49	0.4
LDO (-5V)	MIC5270-5.0YM5	Microchip Technologies	1	1.92	1.45
Reed relay	SIL03-1A72-71D	MEDER electronics	2	3.46	3.14
Battery holder (9V battery)	1295	Keystone electronics	2	3.24	1.96
USB-C cable	3021090-01M	Qualtek	1	5.94	3.47
PCB board 2 layer 8x3cm	N/A	Eurocircuit (low-volume), PCBway (high-volume)		42.85	0.36
Passive components	Various SMD resistors and capacitors		50	0.1	0.03
Copper sheet (0.5mm x 50mm x 1000mm) for shielding	B085VWRBG1	Amazon.es	1	22	7.7
TOTAL				**116.16**	**40.9**

(Acronyms: ADC – Analog-to-Digital Converter, DAC – Digital-to-Analog Converter, LDO – Low-Dropout Regulator, PCB – Printer Circuit Board, SPI – Serial Peripheral Interface)

Table S10. Material cost to prepare disposable RPS chips. This does not include the initial fabrication cost of the reusable Si master mold. hPDMS and Pluronic® F-127 are only used in minuscule amounts and are insignificant for the unit cost of the chip.

Material	Supplier	Package	Cost (EUR)	Number of chips	Unit cost (EUR/chip)
Sylgard 184 PDMS	Farnell	1.1kg	273	550	0.5
hPDMS	Gelest®	100g	205	200k	0.001
Pluronic® F-127	Sigma-Aldrich	250g	115	25M	0.0000046
Glass substrate	RS FRANCE	50pcs	2.78	50	0.06
TOTAL			**596**		**0.56**

11. Comparison of commercially available RPS systems

Up to our knowledge two commercial nanoparticle analyzers based on RPS principle exist currently on the market. One based on tunable RPS (TRPS) and another on microfluidic chip (MRPS), by IZON and Spectradyne, respectively (compared in table S11). In order to achieve full measurement range both products use different cartridges, where each can detect particles within maximum size difference 5 to 8 fold. MRPS has also variant, where RPS is performed simultaneously with fluorescent measurements allowing quantification of surface markers. In all cases particle flow is driven by applied pressure. This work is also based on MRPS approach and has similar features (e.g. being calibration free).

Table S11. Commercially available RPS systems and comparison with this work (* for costs it must be noted, that for commercial devices we described their sales price, while bill of materials (BOM) cost is publicly unknown proprietary information and usually only small fraction of the sales price)

Product	**The Exoid**	**nCS 1 & 2**	**ARC**	**This work**
Manufacturer	IZON	Spectradyne		
Technology	Tunable RPS (TRPS)	Microfluidic RPS (MRPS)	Fluorescent MRPS (F-MRPS)	MRPS
Full size range	40 nm - 11 µm	50 nm - 10 µm		~80 nm-900 nm
Size range/cartridge	5-7x	6-8x		4-5x size ranges detected in single measurement
Sizing precision	Not specified	~ ±5%		~8% from nominal values
Sample volume	Not specified	2-3 µL		~10 µL
Cartridge selection	9 size ranges	5 size ranges		2 selected pore sizes
Flow mechanism	Pressure			
Z-potential measurement	Yes	No	No	No
Fluorescence measurement	No	No	Yes (one excitation and 3 simultaneous emission channels)	No
Concentration range	10^5-10^{11} /mL depending on size	10^4-$5x10^{11}$ /mL depending on size 2000-50'000x per cartridge		$3x10^6$-$3x10^{10}$ /mL were tested depending on the chip
Detection rate	Not specified	10 kHz		10-100 spikes/s sampling up to 100 kHz
Requires calibration with standard	Yes	No	No	No
Other features	Easier to unclog. Possible to change samples. Requires calibration. Tunable pore size.	Faster to measure without calibration. Integrated filters to minimize clogging risk. More reproducible without user adjustable measurement settings.		Possible to change solution. Calibration free.
Instrument cost*	42'900 EUR	>50'000 USD	>150'000 USD	~3´400 EUR (with DAQ card) and <170 EUR (after optimization as described in SI section 10)
Cartridge/chip cost*	19 EUR + calibration particles	10-15 USD (both use same chip)		0.56 EUR (chip material cost)

12. References

[1] W. Hellmich, J. Regtmeier, T. T. Duong, R. Ros, D. Anselmetti, and A. Ros, *Langmuir*, **2005**, 16, 7551-7557.

[2] Mariscal, J.; Fernandez-Puente, P.; Calamia, V.; Abalo, A.; Santacana, M.; Matias-Guiu, X.; Lopez-Lopez, R.; Gil-Moreno, A.; Alonso-Alconada, L.; Abal, M. Proteomic Characterization of Epithelial-Like Extracellular Vesicles in Advanced Endometrial Cancer. *J. Proteome Res.* **2019**, 18, 1043–1053.